Science and Technology of Advanced Materials

ISSN: (Print) (Online) Journal homepage: https://www.tandfonline.com/loi/tsta20

Combinatorial treatment using bevacizumab/pemetrexed loaded core-shell silica nanoparticles for non-small cell lung cancer

Deepika Radhakrishnan, Vaishwik Patel, Shan Mohanan, Sharon Wong, Jacob Netherton, Ajay Karakoti & Ajayan Vinu

To cite this article: Deepika Radhakrishnan, Vaishwik Patel, Shan Mohanan, Sharon Wong, Jacob Netherton, Ajay Karakoti & Ajayan Vinu (26 Oct 2023): Combinatorial treatment using bevacizumab/pemetrexed loaded core-shell silica nanoparticles for non-small cell lung cancer, Science and Technology of Advanced Materials, DOI: 10.1080/14686996.2023.2274819

To link to this article: https://doi.org/10.1080/14686996.2023.2274819

Publisher: Taylor & Francis & The Author(s). Published by National Institute for Materials Science in partnership with Taylor & Francis Group.

Journal: *Science and Technology of Advanced Materials*

DOI: 10.1080/14686996.2023.2274819

Combinatorial treatment using bevacizumab/pemetrexed loaded core-shell silica nanoparticles for non-small cell lung cancer

Deepika Radhakrishnan[1], Vaishwik Patel[1], Shan Mohanan[1], Sharon Wong[1], Jacob Netherton[2], Ajay Karakoti[1], Ajayan Vinu[1]*

[1]*Global Innovative Center for Advanced Nanomaterials, The University of Newcastle, Callaghan, Australia*

[2]*School of Biomedical Sciences and Pharmacy, The University of Newcastle, Callaghan, Australia*

Contact: Ajayan Vinu: Ajayan.Vinu@newcastle.edu.au, Global Innovative Center for Advanced Nanomaterials, The University of Newcastle, Callaghan, Australia

Combinatorial treatment using bevacizumab/pemetrexed loaded core-shell silica nanoparticles for non-small cell lung cancer

Non-small cell lung cancer (NSCLC) is a life-threatening cancer associated with a higher mortality rate. Despite promising results shown by combination therapies, there remains a need for efficient drug delivery materials capable of combining various drugs, imaging agents, and targeting agents to enhance treatment efficacy. In this study, we present the synthesis of novel core-shell hollow mesoporous silica nanoparticles (@MSN) with bimodal porosity and a large surface area (694 m^2/g) to facilitate targeted drug delivery for NSCLC treatment. The hollow core-shell structure enables the loading of a substantial quantity of the pemetrexed drug, up to 839 µg/mg, with a sustained release of 20% within 48 hours. The MSN is surface functionalised with amino and carboxyl groups to accommodate an imaging agent and facilitate the attachment of the targeting drug bevacizumab. These particles exhibit rapid uptake by both A549 and PC-9 cells. Moreover, the targeting by bevacizumab leads to higher cytotoxicity within 48 hours and induces apoptosis more effectively than the non-functionalised samples. As a versatile drug delivery platform, the hollow core-shell MSN demonstrated in this study holds great potential for various drug delivery applications.

Keywords: Non-small cell lung cancer (NSCLC); combinatorial treatment; core-shell silica nanoparticles

1. Introduction

Lung cancer stands as one of the most frequently diagnosed cancer type in all over the world, with a high occurrence and mortality rate. In the year 2020 alone, over 2.2 million new diagnosis and 1.7 million deaths were registered worldwide [1]. Non-small cell lung cancer (NSCLC) is most common, comprising more than 85% of total cases and carrying the maximum disease burden. Several advanced therapies have been developed to tackle NSCLC, including a new generation of drugs targeting important pathways to block disease progression [2,3]. For example, therapies targeting the epidermal growth factor receptor (EGFR), PI3K/AKT/mTOR, mitogen-activated protein kinases (MAPKs), and neurotrophic tyrosine receptor kinase (NTRK)/c-ros

oncogene (ROS1) pathways have been developed for lung adenocarcinoma treatment [4-11]However, despite the promising results, targeted therapy is usually restricted to patients with certain genetic mutations. In some cases, multiple mutations can be present, and tumours also eventually become resistant to the targeted drugs over time [12-14]. Several clinical trials which assessed the combination of targeted therapy with chemotherapy have showed reasonable success [15]. For instance, bevacizumab (BEV), a VEGF-targeting anti-angiogenesis drug, combined with chemotherapeutic drugs like cisplatin and paclitaxel have shown promising clinical results [16,17]. Nonetheless, side effects persist for these combinatorial treatments due to the non-specificity of the chemotherapeutic drugs, and their overall toxic effect[18]. Thus, the encapsulation of drugs within a nanoparticle-based delivery is warranted for targeted drug delivery since nano drug delivery carriers have increased permeation and retention (EPR) effect which increases drug availability in tumours due to leaky vasculature compared to normal cells [19,20].

The encapsulation and delivery of drugs from carriers, such as liposomes, polymers, and mesoporous silica nanoparticles (MSN), represent an appealing strategy for diverse cancer therapies. This approach aims to mitigate drug side effects and enhance their effectiveness. MSNs have gained significant attention as alternate drug carriers to liposomes owing to their remarkable textural properties, ordered porous structure, chemical stability, tunable surface chemistries, high biocompatibility, and established clearance from the body [21-25]. Besides, the adsorption capacity of these high surface area silica or other porous hybrid nanoparticles is remarkable and well-studied [23,24,26-28]. Notably, core-shell MSNs have further tunable textural properties in the inner core distinct from the outer shell [24,29]. For instance, a study conducted by *Rong et al*, reported the incorporation of the drug bortezomib into the mesopores of the core,

coupled with the attachment of P53 targeting genes onto the surface of the shell in mesoporous silica nanoparticles. By harnessing both the core and shell components, the research team showcased a promising mechanism for the utilization of core-shell silica nanoparticles in lung cancer treatment [30]. Other than the core-shell silica NPs, an enhanced effect of the chemotherapeutic drug pemetrexed in human breast cancer cell line SKBR3 (Isolated by the Memorial Sloan- Kettering Cancer Centre in 1970) with overexpresses Her2 has been reported after loading the drug over the functionalised SBA-15 [31]. Some of the very limited studies on the core-shell silica NPs loaded drug paclitaxel have also been noted [32]. Furthermore, core-shell nanoparticles exhibit superior biocompatibility, dispersibility, and improved compatibility with biomolecules, like MSNs. These characteristics facilitate their application in drug delivery [33].

In recent times, the utilization of diverse block copolymers has enabled the achievement of a bimodal mesoporous structure in MSNs, characterised by precisely defined pore arrangements. The advantage of bimodal porosity is that it can enable the loading of two different drugs, as often the case in combinatorial therapy, within the same material based on size exclusivity [34,35]. This reduces the need to give two different and independent treatments for two drugs. Having drugs loaded in different compartments also prevents drug-drug interactions. Bimodal porosity can also facilitate loading imaging agents and other molecules along with chemotherapy or immunotherapy drugs. Loading these molecules in different porous compartments will reduce their effect on the drug loading capacity. Even though achieving a core-shell structure with tunable core and shell properties and bimodal porosity is advantageous, their synthesis is extremely challenging and requires the careful design and use of multiple templating agents. Limited studies have shown the application of bimodal mesoporous silica NPs in NSCLC to deliver either the peptides or the genes [36]. Sundarraj et al. reported an

enzyme-targeted combinatorial therapy with the chemotherapeutic drug and the EGFR antibodies in lung cancer cells using core-shell MSNs [37]. But, other than this promising research, reports on combinatorial therapy in lung cancer using core-shell silica nanoparticles are scarce. Given the promise of combinatorial therapy in NSCLC treatment, it is important to derive strategies and materials for delivering a combination of drugs for NSCLC treatment. Developing bimodal core-shell silica NPs, which can accommodate different types of drugs and/or imaging agents by tuning the pore sizes and potentially targeting the cancer cells by functionalising the surface of the NPs, could become promising drug delivery materials for NSCLC treatment.

In this study, we present a robust method for synthesising core-shell mesoporous silica nanoparticles (@MSN) with a bimodal pore size distribution. This was achieved by using three distinct surfactant systems, employing a combination of vesicle and dual liquid crystal templating approaches. This innovative technique establishes a promising platform for drug delivery in the context of lung cancer treatment. The core of these nanoparticles is formed from a triblock copolymer known as Pluronic F127, while the mesoporous shell is created through the interaction between cetyltrimethylammonium bromide (CTAB) and silica species. Additionally, the introduction of fluorocarbon (FC-4) was employed to regulate particle size and shape. The resulting materials exhibited ordered mesoporous structure, characterised by bimodal pores, a distinctive core-shell configuration, and a spherical morphology. Notably, these materials possess a substantial specific surface area and a considerable volume of mesopores. To enhance both targeting and controlled release of the chemotherapeutic drug pemetrexed, a monoclonal antibody known as bevacizumab was functionalised onto the surface of these novel core-shell MSNs. This strategic modification aims to elevate the efficacy of these drugs for lung cancer treatment.

2. Materials and methods

2.1. Materials

All the chemicals except the cationic fluorocarbon surfactant FC-4 ($C_{20}H_{20}F_{23}IN_2O_4$) and cell culture media were purchased from Sigma–Aldrich. FC-4 was obtained fromYick-Vic Chemicals.

2.2. Synthesis of hollow core-shell mesoporous silica nanoparticles using Pluronic F127, CTAB and FC-4

Hollow core-shell MSN was synthesised in a strongly alkaline medium using a triple surfactant system. In the typical synthesis, 0.1 g of Pluronic F127 and 0.2 g of FC-4 were dissolved in 20 mL of tetrahydrofuran (THF) and stirred at 30^{o}C for 30 minutes (suspension 1). Simultaneously, 0.1 g of CTAB was dissolved in a solution of 3 mL of NH_3 and 80 mL of H_2O, and stirred at 35°C for 30 minutes (suspension 2). The two suspensions were combined by adding suspension 2 to suspension 1, followed by 45 minutes of stirring at 30°C. Then, 160 mL of ethanol was added and stirred for 3 hours followed by the addition of 0.6 g of TEOS with the continuous stirring for an additional 24 hours. The mixture was aged at 100°C for 24 h and centrifuged at 4500 rpm for 10 minutes after cooling, and dried at 100°C. The dried samples were calcined at 550°C for 24 hours [38]. The impact of FC-4 on the size and morphology of the MSN was assessed by varying the FC-4 concentration, denoting these samples as @MSN-xF, where x represents the amount of FC-4 used for synthesis. Finally, the calcined powder was collected and gently ground before undergoing characterization.

2.3. Surface functionalization of core-shell mesoporous silica nanoparticles

Synthesis of both amine (NH_2@MSN) and carboxyl functionalised (NH_2@MSN-CO) core-shell MSN was achieved on the optimised @MSN-0.2F by adapting the post-

synthetic grafting method of Zhang et al. [39]. At first, the samples were coated with APTES by dispersing 100 mg of @MSN-0.2F sample in 20 mL anhydrous toluene, followed by the addition of 100 μL APTES with constant stirring. The mixture was then refluxed for 12 hours at 100 ℃ and cooled down to room temperature. The suspension was filtered, washed with toluene and dried at 60 ℃ in a vacuum oven overnight [39]. The sample is denoted as NH_2@MSN-0.2F. For carboxyl functionalization, the mixture that had undergone reflux with APTES was supplemented with 80 μL of CTES and then refluxed at 100°C for an additional 24 hours. Following this step, the suspension was cooled, washed, and dried, resulting in a product denoted as NH_2@MSN-CN. Subsequently, 250 mg of NH_2@MSN-CN was dispersed in 40 mL ethanol and stirred for 5 minutes. After the addition of 50% sulfuric acid (v/v), the mixture was refluxed, washed and dried. This final product is referred to as NH_2@MSN-CO.

2.4. Physico-chemical characterization

The structure of the @MSN was analysed by using a Panalytical Empyrean XRD instrument (Generator Voltage 40 kV; Tube current 40 mA; Divergence slit 1/16°; Scan rate 0.0017 ° sec^{-1}). Textural characteristics of all samples were assessed through nitrogen adsorption experiments by using a Micromeritics ASAP 2420 instrument. Surface morphology and @MSN size were investigated using a JEOL 7001 field emission scanning electron microscopy (SEM) at 10 kV. Transmission electron microscopy (TEM) images were acquired with a JEOL 2100 instrument. Fourier transform infrared (FTIR) spectra of the pristine and functionalised MSN were collected using Perkin Elmer Frontier. The thermal decomposition behaviour of both pristine and functionalised MSN samples was studied using a Perkin Elmer thermogravimetric analyser (Model no. STA-8000).

2.5. Fluorescein isothiocyanate (FITC) labeling of mesoporous silica nanoparticles

A solution of 10 mL of ethanol containing 2 mg of FITC was prepared. Subsequently, 5 mg of NH_2@MSN-CO was introduced into the FITC solution, and stirred for 24 hours at room temperature under light protection. Following the 24-hour period, the resulting, yellow-coloured nanoparticles were separated through centrifugation at 19000 rpm for 20 minutes. The separated nanoparticles underwent two rounds of washing using ethanol. Finally, the powdered samples were collected and subjected to freeze-drying for subsequent studies [40].

2.6. Loading of pemetrexed onto FITC-labelled mesoporous silica nanoparticles

The FITC-labelled, pristine, and functionalised @MSN samples were preheated under vacuum at 100°C and 40°C, respectively, for 24 hours to eliminate any moisture. 8.3 mg/mL stock solution of pemetrexed was prepared using 20% v/v ethanol. Subsequently, 25 mg of pristine and functionalised @MSN were dispersed and immersed in 6 mL of the prepared solution. This mixture was subjected to continuous gentle stirring at 37°C for 24 hours to reach equilibrium. The samples were subjected to filtration, repeated wash with water and freeze-drying. These respective samples were designated as PEM@MSN, PEM@MSN-NH, and PEM@MSN-NHCO. To quantify the amount of pemetrexed adsorbed, the absorbance of the remaining supernatant at 226 nm was measured. The functionalization of bevacizumab involved suspending 100 mg of pemetrexed-loaded MSN in MES buffer (pH 6) to initiate the EDC/NHS reaction. After washing the MSN with PBS, 100 µL of bevacizumab antibody at a molar ratio of 10:1 was added. This mixture was incubated for 6 hours at room temperature and separated through centrifugation.[41]

2.7. In vitro drug release studies

The release of pemetrexed from the prepared @MSN was investigated in two distinct pH media at 37°C: acetate buffer (pH = 5.5) and phosphate-buffered saline (pH = 7.4). 5 mg of samples were suspended in the chosen buffer and enclosed within a dialysis bag (MWCO – 8000 Daltons). These bags were then positioned in 12.5 mL of the corresponding release medium, while maintaining continuous stirring at 100 rpm at 37°C. To comprehend the kinetics of drug release, the quantity of released drug was assessed using UV-Vis spectrophotometry at 226 nm at various time intervals: 3, 6, 12, 18, 24, 36, and 48 hours.

2.8. Cell culture

A549 and PC-9 lung adenocarcinoma cell lines were cultivated under humidified conditions of 37°C, 5% CO_2. For the A549 cell line, the growth medium employed was DMEM/F12 (Sigma D0697), while RPMI 1640 was utilised for the PC-9 cell line. Both media were supplemented with 10% fetal bovine serum (FBS) and 1% streptomycin and penicillin. Routine medium replacement was carried out for both cell lines every other day, while ensuring proper care and attention.

2.9. Cellular uptake of pemetrexed-loaded MSN

2.9.1. *Flow cytometry*

A549 and PC-9 cells were seeded into two different 96-well plates and incubated for 24 hours. Subsequently, the cells were exposed to 50 µg/mL to 300 µg/mL @MSN for 6 and 12 hours. For cellular uptake studies, FITC-labelled amine and carboxyl functionalised @MSN were employed. These cells were seeded and incubated at 37°C. Cells that did not receive any treatment were utilised as the control group. After

trypsinization, the cells were washed with PBS, followed by resuspension in PBS. The collected cells were subjected to analysis using a flow cytometer.

2.9.2. *Confocal fluorescence microscopy*

A549 and PC-9 cells were seeded onto glass coverslips. After 48 hours, the cells were treated with 200 µg/mL of PEM@MSN, PEM@MSN-NH, PEM@MSN-NHCO, and BEV-PEM@MSN. At 3-, 6-, and 12-hours post-treatment, the cells were subjected to incubation with the Cell Plasma Membrane Staining Kit (abcam, ab138892) for a duration of 20 minutes. Following staining, the cells underwent several washes with PBS and were then fixed using 4% paraformaldehyde. Subsequently, the cells were mounted using ProLong™ Gold Antifade Mountant with DAPI (Invitrogen), and imaging was performed utilising a Zeiss LSM 900 confocal microscope. This imaging was carried out to ascertain the time-dependent uptake of @MSN within the cells.

2.10. Cellular apoptosis

After the cells were seeded and the following a 48-hour incubation period, the cells were subjected to treatment with 200 µg/mL of PEM@MSN-NHCO and BEV-PEM@MSN for a duration of 12 hours. Subsequently, the cells were trypsinised and exposed to Annexin V-FITC isomer (5 µL) and Propidium Iodide (PI, 5 µL) in 500 µL binding buffer at room temperature for 15 minutes, away from light. For comparison, untreated cells served as the control. The details of the interpretation of the results are given in the supporting information.

2.11. In vitro cytotoxicity

The cytotoxic impact of drug-loaded MSN samples on A549 and PC-9 cells was evaluated using the MTT assay. After the cells were seeded into a 96-well plate, the cells were treated with 100 µg/mL to 500 µg/mL of PEM@MSN, PEM@MSN-NH,

PEM@MSN-NHCO, and BEV-PEM@MSN, each in 100 µL of culture media. After an incubation period (24 to 48 h), MTT solution was added. The cells were then subjected to further incubation at 37°C and 5% CO_2 for 4 hours. Following this, 100 µl of dimethyl sulfoxide (DMSO, Sigma-Aldrich) was introduced to each well, and the absorbance at 590 nm was measured.

3. Results and discussion

3.1. Characterization of @MSN-xF particles

@MSN was synthesised using a triple surfactant approach, wherein the amount of pluronic F127 and CTAB were kept constant at 0.1g and 0.2g respectively while varying amount of FC-4 was used, ranging from 0 to 0.5 g. To investigate FC-4's impact on the structural order and morphology, all prepared samples were analysed by HR-SEM, HR-TEM and low angle powder X-ray diffraction measurements. HR-SEM images showed that all @MSN-xF samples display spherical particles regardless of the concentration of FC-4 but are of different sizes (**Figure 1A-F**). Notably, monodisperse spherical particles were only observed when the amount of FC-4 was increased from 0 to 0.2 g. With further increase of the FC-4 above 0.2 g, spherical particles of variable sizes were observed with sporadic occurrence of particles with fiber-like morphology. The particle size of @MSN-0F was within the size range of 300-690 nm, decreasing to 250-320 nm for @MSN-0.1F (**Figure 1A-B**). The particle size for @MSN-0.2F was slightly increased but remained in the range of 300-330 nm (**Figure 1D**). The considerable reduction in particle size compared to @MSN-0F may be attributed to the presence of hydrophobic fluoride moieties, which help to repel the surfactant-silica self-assembled structures, resulting in the formation of small particles. Although the particle size of @MSN-0.1F and @MSN-0.2F were almost similar, the shape of the former was

less uniform with some elongated structure observed. With increasing FC-4 above 0.2 g, particle size was significantly increased to the range of 320 nm to 1820 nm (**Figure 1E-F**). For @MSN-0.5F, spherical particles with irregular sizes and agglomeration were observed. This may be attributed to the domination of FC-4 in the synthesis mixture, which not only forms the spherical micelles but also interact with pluronic F127 to create large spherical micelles, resulting in uneven distribution of spherical particles and aggregation. Among the samples prepared, @MSN-0.2F had monodisperse nanosphere particles with uniform size and shape. Of note, HR-SEM images of broken particles demonstrated that the centre was hollow (arrow in **Figure 1A**), confirming the formation of empty core-shell MSN.

The formation of mesopores on the shells of the spherical particles for @MSN-0.2F and @MSN-0F were confirmed in their HR-TEM images (**Figure 2A-F**). @MSN-0.2F exhibited only monodisperse spherical particles without any fiber-like structure (**Figure 2D-F**). In contrast, the images of @MSN-0F displayed a large amount of non-porous silica fibers surrounding the spherical particles (**Figure 2A-C**), which is in close agreement with the HR-SEM images observed for samples prepared with and without FC-4. These results reveal that the addition of FC-4 controls the size and shape of the core shell nanoparticles.

Characterization of @MSN-xF samples through low-angle powder X-ray diffraction (XRD) showed a broad peak at a lower angle (**Figure 3A**). This could be attributed to (100) reflection of the hexagonal space group p6mm suggesting the presence of mesopores within the shell walls of @MSN. Intriguingly, peak intensity grew proportionally with increased FC-4 in the synthesis mixture, ranging from 0.1g to 0.5g. This trend indicates that the addition of FC-4 enhances the structural order of @MSN-xF. Notably, the full-width half maximum (FWHM) of the peaks in @MSN-xF also

expanded as FC-4 quantity increased during synthesis. This may be attributed to the reduction in the scattering domain size or a slight disorder in the mesostructure. There was also a clear correlation between the FWHM of the peak and the particle size of the @MSN-xF samples. Among the samples studied, @MSN-0.1F has the smallest FWHM and the smallest particles. The calculated unit cell length based on the d-spacing of the samples underwent changes. With an increase in FC-4 from 0g to 0.2g, the unit cell length rose from 4.24nm to 4.54nm, subsequently decreasing to 4.25nm as FC-4 was further elevated to 0.5g.

The textural characteristics of the @MSN-xF were investigated using nitrogen adsorption-desorption isotherms. All samples displayed type VI isotherms with H4 hysteresis as per the latest IUPAC classification (**Figure 3B**). Based on the shape of the isotherms, the prepared samples exhibited bimodal pores, which are generated due to the multiple surfactants used. The isotherms of all the samples displayed an H4 hysteresis loop, which may be attributed to the presence of ink-bottle-shaped pores (small pore entrances connected to large cavity at the centre), suggesting the presence of empty core-shell with ordered mesopores in the samples. All samples had bimodal pores regardless of the presence of FC-4 (**Figure 3C, Table 1**). Interestingly, the size of the larger pores of @MSN-xF decreased upon the addition of FC-4. The decrease in size can be attributed to the relatively weak interaction between CTAB and F127, as FC-4 covers the surface of F127 micelles surface. Additionally, the introduction of FC-4 into the system might disrupt the self-assembly between CTAB and FC-4 but promote its interaction with F127. This interaction could result in a reduction in pore size. The specific surface area and pore volume of the samples fall within the range of 654 to 710 m^2/g and 0.4 to 0.6 cm^3/g, respectively **(Table 1)**. The large specific surface area is primarily a consequence of the mesopores within the wall structure of the @MSN

samples. These mesopores form through the straightforward self-assembly process involving TEOS and CTAB micelles, along with subsequent assembly on the surface of F127 and FC-4 spherical micelles.

The optimised sample, @MSN-0.2F, which exhibited spherical particles within the size of 300-330 nm, was selected for subsequent drug adsorption and delivery studies. Before the adsorption of drugs, @MSN-0.2F was functionalised with amine and carboxyl groups using previously reported methods [39]. The functionalised @MSN-0.2F were characterised by FTIR spectroscopy, CHN analysis **(Table S2)**, and thermogravimetric analysis (TGA). The amine functionalised @MSN-0.2F (NH_2@MSN) showed a nitrogen content of 2.92 wt%, which was reduced to 1.96 wt% for carboxyl functionalised sample (NH_2@MSN-CO). Similarly, the weight percentage of carbon and hydrogen were also reduced from 7.52 to 5.37 wt% and from 2.32 to 1.76 wt% respectively. TGA results showed a large mass change in the functionalised NH_2@MSN-0.2F and NH_2@MSN-CO when compared to the pristine @MSN-0.2F (Figure 4A). This observation was validated by the changes in FTIR spectra (**Figure 3D**). All @MSN-0.2F samples have shown the stretching vibration at 3426 cm^{-1}. indicating the presence of hydroxyl group. The peaks related to deformation and stretching vibration of Si-OH were observed at 1656 cm^{-1} and 985 cm^{-1} respectively for @MSN-0.2F, indicating the presence of numerous silanol groups in the unfunctionalised samples. In NH_2@MSN, the characteristic Si-OH stretching vibration was absent, and the hydroxyl group's stretching vibration at 1656 cm^{-1} was reduced. Bands at 2970 cm^{-1} and 2926 cm^{-1} were attributed to the -CH_2 groups of APTES, confirming the surface functionalization of silanol groups with APTES molecules. The FTIR spectra also confirmed carboxyl group functionalization, as the initial cyanine (CN) stretching band at 2257 cm^{-1} was successfully replaced with -COOH at 1734 cm^{-1}

for NH_2@MSN-CO. This change indicated the successful modification of both carboxyl and amine groups on the @MSN [39].

3.2. Drug adsorption and release in @MSN-0.2F particles

Pemetrexed is a folate antimetabolite that is considered the first-line chemotherapeutic drug in advanced NSCLC treatment [42-44], hence it was loaded onto the three MSN preparations (@MSN-0.2F, NH_2@MSN and NH_2@MSN-CO) in this study. @MSN-0.2F demonstrated the highest drug loading capacity, adsorbing 839 µg/mg of pemetrexed as measured using UV-Vis spectroscopy. Drug loading capacity was slightly lower in the NH_2@MSN and NH_2@MSN-CO, at 823 µg/mg and 670 µg/mg respectively (**Figure 4B**). This is likely due to the loss of surface area following their functionalization with amine and carboxyl functional groups (**Table S1**). Nonetheless, NH_2@MSN-CO recorded the highest drug loading capacity when normalised against surface area (3454 ng/m^2), followed by NH_2@MSN (2064 ng/m^2) and the pristine @MSN-0.2F (1232 ng/m^2) samples. It's noteworthy that the drug loading capacity of NH2@MSN-CO, per unit surface area, surpasses that of @MSN-0.2F by more than 2.5 times. Thus, it can be inferred that even though functionalization with amine and carboxyl groups reduced the surface area substantially, the functional groups did not occlude the pores for loading drug molecules. More importantly, the presence of functional groups facilitated higher drug adsorption, likely through the promotion of hydrogen bonding interaction between pemetrexed and the carboxyl and amine functional groups in MSN. After drug loading, the samples are referred to as PEM@MSN, PEM@MSN-NH and PEM@MSN-NHCO.

Drug loading capacity was also determined using TGA which measures the extent of weight loss caused by decomposition of drug when heated to 700 ^oC. The percentage weight loss was observed to be in the order of PEM@MSN-NH ≈ PEM@MSN>

PEM@MSN-NHCO, which followed the same trend as the drug loading capacity obtained from UV-Vis absorption measurements (non-normalised) (**Figure 4A**). Both PEM@MSN-NH and PEM@MSN samples showed nearly 45-48% weight loss, while PEM@MSN-NHCO depicted a weight loss of about 32%. The control samples of @MSN-0.2F, NH_2@MSN and NH_2@MSN-CO showed less than 10% weight loss, confirming that the weight loss observed in drug-loaded samples was ascribed to pemetrexed. Given PEM@MSN-NHCO showed a good drug loading capacity (highest per unit surface area), it was used to attach bevacizumab, denoted as BEV-PEM@MSN-NHCO.

Pemetrexed released from all MSN samples was assessed in phosphate-buffered saline (PBS) at pH 7.4 and acetate buffer at pH 5.5, mimicking the microenvironment of normal and cancer cells, respectively. As observed in **Figure 5A-B**, an overall slow and sustained release of pemetrexed was observed for all samples in both acidic and neutral medium. The slow release can be attributed to the pore geometry, characterised by having a large core with small opening(s). The low solubility of pemetrexed in aqueous media[45] likely also reduces its release into both media. At pH 7.4, a more rapid initial release occurred for all samples within the first 6 hours, followed by a more gradual release trend **(Figure 5B)**. This behaviour can be attributed to the initial release of pemetrexed that was weakly adsorbed on the surface of the @MSN particles. By the 12-hour mark, approximately 15% of pemetrexed was released from PEM@MSN, while only 9% was released from PEM@MSN-NH, as compared to approximately 12% for PEM@MSN-NHCO and BEV-PEM@MSN. The comparatively lower release from the functionalised samples can be attributed to two factors: a) the stronger interaction between the functional amine/carboxyl groups and pemetrexed, as documented in previous studies [31], and b) the hindrance of pemetrexed release by bevacizumab on

the surface of MSN. Overall, the cumulative drug release from all samples within the 48-hour timeframe at pH 7.4 ranged between 15-20%.

Under acidic conditions at pH 5.5, the drug release profile was distinct to those at pH 7.4. The highest overall drug release was observed in PEM@MSN-NHCO (18%) ≈ BEV-PEM@MSN, followed by PEM@MSN-NH (14%) and PEM@MSN (12%). As expected, the PEM release from the functionalised sample was higher than bare MSN due to the protonation of the amine groups that reduced the interaction between the amine groups and the PEM. Despite protonation in acidic pH, the drug release was lower. Almasi et al. reported that a similar slower release of the amine and thiocyanate functionalised SBA-15 (Santa Barbara Amorphous-15) samples attributed to the stronger interaction between the amine and the carboxyl groups and the PEM [31]. The overall lower drug release observed in acidic pH can also be ascribed to the surface polarity of the MSN as well as the protonation of pemetrexed, which reduces its solubility. The dissolution kinetics of the silica is also slower in acidic pH thereby further reducing drug release [46]. Thus, it can be confirmed that the MSN samples depict a high affinity for the drug PEM and by comparing the drug release rate at two pH values, the drug encapsulated showed a sustained release from the functionalised MSN. Since all four samples showed robust drug loading capacity and sustained drug release, they were further tested for their efficacy on lung cancer cells.

To study the potential of the drug-loaded MSN as a drug delivery agent, the cell viability in response to the drug-loaded particles was tested in two lung adenocarcinoma cell lines, A549 and PC-9. At first, the cell viability of bare and functionalised samples @MSN-0.2F was tested, and it was found that all the samples were tolerated by both A549 and PC-9 cells at as high dose as 500 µg/mL for 24 hours (**Figure 6A, C**). However, the cell viability decreased in both A549 and PC-9 after 48 h incubation with

bare particles (**Figure 6B, D**). The dose-dependent toxicity of bare particles in A549 cells was nearly 30% at the highest concentration of 500 µg/mL. PC-9 cells were more sensitive to the bare particles which have a surface charge of -21.6 mV, with more than 50% cell death observed for @MSN-0.2F and NH_2@MSN at all concentrations tested in this study. The high positive charge of NH_2@MSN (+34 mV) can lead to the observed high cytotoxicity of these particles. However, NH_2@MSN-CO with a slightly lower surface charge (+26 mV) was well-tolerated by PC-9 cells, showcasing over 60% cell viability even at the highest dose of 500 µg/mL. The surface charge has been shown to affect the internalization and disrupt the cell membranes of the cells and could influence the cytotoxicity observed for bare particles after 48 h of incubation with cells [47,48].

The cell response to pemetrexed-loaded MSN after 24 and 48 hours of incubation was also analysed (**Figure 6E-H**). Dose-dependent cytotoxicity was evident across all samples following 24 and 48 hours of incubation in both cell lines. It was also observed that drug-loaded nanoparticles caused a much higher cytotoxicity than bare particles at all concentrations tested in this study, suggesting that the particles successfully released pemetrexed inside the cells. Among different samples, the highest cytotoxicity was observed for PEM@MSN-NH and BEV-PEM@MSN at 500 µg/mL after 24 h of treatment whereas BEV-PEM@MSN registered the highest cytotoxicity after 48 h treatment in both PC-9 and A549 cells, suggesting that BEV functionalised particles show slightly better cytotoxicity as compared to PEM@MSN-NH after long term incubation.

To confirm that the increased cytotoxicity of the drug-loaded particles is due to the drug release from the internalised MSN, we analysed the uptake of MSN using flow cytometry and confocal imaging. NH_2@MSN-CO sample (as a representative of all

MSN samples) was functionalised with FITC for flow cytometry analysis and incubated with A549 and PC-9 cells for 24 h. The increase in the fluorescence intensity from the cells treated with FITC-labelled particles was used for evaluating the uptake of the particles. No fluorescence signal was observed for untreated A549 cells (**Figure 7A)**. However, cells treated with FITC labelled NH_2@MSN-CO showed a dose-dependent increase in fluorescence intensity (**Figure 7B-F**). It was also found that the number of cells with higher fluorescence intensity increased steadily with increasing concentration of the particles, suggesting a higher uptake of the particles by the cells. Similar observations were made for uptake in PC-9 cells (**Figure S3**), indicating that the NH_2@MSN-CO particles were internalised in both cells within 24 h of treatment.

Further confirmation of the nanoparticle uptake by the cells was obtained using confocal imaging of A549 cells treated with FITC labelled BEV-PEM@MSN. The representative confocal microscopic images in **Figure 8** showed that the BEV-PEM@MSN particles were internalised in a time-dependent manner, and the in A549 cells was completed within 12 h. The internalization was minimal within the first 3 hours, as observed by a weak fluorescence from the FITC labelled particles. However, strong fluorescence was observed within 6 hours, increasing further after 12 h incubation. From the confocal images, it is noted that large clusters of MSN are observed in the cytoplasm at 6 and 12 h. It is also clear that the particles were not present within the nucleus until 12 h. Based on the flow cytometry and the confocal imaging data, it can be inferred that the prepared MSN particles herein can be internalised within both PC-9 and A549 cells[42-44].

Pemetrexed has been shown to induce cellular apoptosis following multiple pathways, but the exact mechanism of cycle arrest has been debated [44,49]. While bevacizumab (BEV) is an anti-angiogenic drug that targets and selectively binds to the VEGF to

check uncontrolled angiogenesis in tumours, in this study, BEV is functionalised on the outer surface of the functionalised @MSN in low concentration only to target the VEGF receptors and enhance the therapeutic efficiency of the PEM loaded core-shell MSN. Thus, the functionalization of the BEV is not at the therapeutic level and is expected to influence the cytotoxicity of the PEM by targeting the MSN and influencing the uptake. To understand the effect of BEV functionalization in targeting overexpressed VEGF receptors, PEM-induced cellular apoptosis was analysed by using flow cytometry in A549 cells. Figure 9 compares the flow cytometry data from the A549 cells treated with 200 µg/mL of PEM@MSN-NHCO and BEV-PEM@MSN samples for different duration of time. It was observed that PEM@MSN-NHCO induced apoptosis in A549 cells within 6 h. BEV-PEM@MSN showed significantly higher apoptosis than PEM@MSN-NHCO at both 6 h and 12 h. The percentage of total apoptotic cells (combined early and late apoptosis) was greater than 85% for BEV-PEM@MSN treated cells at both time-points as compared to PEM@MSN-NHCO, which shows only >50% apoptotic cells in 6 h and less than 10% in 12 h (Figure 9C). The reduction in the apoptotic cell percentage in only PEM-treated cells can be ascribed to the natural proliferation of the A549 cells with time. It also suggests that PEM release from PEM@MSN-NHCO is below the therapeutic level, probably because of lower internalization or drug release outside the cells as compared to BEV-PEM@MSN. Thus, the targeting action of BEV helps to deliver a higher concentration of PEM and induce cellular apoptosis more efficiently for BEV-PEM@MSN.

4. Conclusions

This study reported a novel synthesis approach for the fabrication of hollow core-shell MSN with bimodal porosity using a triple surfactant-assisted soft templating method. The use of fluorocarbon FC-4 surfactant to control the size and introduce bimodal

porosity was evaluated, and it was found that size, ordered structure and surface area can be controlled by tuning the concentration of FC-4. MSN within the size range of 250 – 330 nm with a high surface area were synthesised and functionalised with both amine and carboxyl groups to facilitate the attachment of targeting drug bevacizumab on the surface along with an imaging agent. The hollow core-shell structure with bimodal porosity resulted in high pemetrexed adsorption (839 µg/mg) in bare MSN owing to a high surface area and hollow core. However, the adsorption per unit surface area was higher for amine functionalised MSN due to stronger interaction between the amine groups and the drug molecules. The drug release was lower than 20% in 48 h for all the samples, probably due to the pore geometry with a large core and small opening. Flow cytometry and confocal imaging confirmed that the NH2@MSN-CO and BEV-PEM@MSN were internalised within 12 h. The cytotoxicity analysis showed that both PEM@MSN-NH and BEV-PEM@MSN exhibited high cytotoxicity as compared to PEM@MSN and PEM@MSN-NHCO in both A549 and PC9 cells despite only 20% drug release was attained. The apoptosis analysis, however, showed that BEV functionalization helps in inducing higher apoptosis in A549 samples as compared to PEM@MSN-NH alone, suggesting that s. The generic nature of this hollow core-shell silica system with bimodal porosity is applicable for drug delivery in a range of different cancers.

5. Acknowledgement

The authors acknowledge Dr. K. Ramadass, Dr. C.I. Sathish, Dr. Nicole Cole, Dr. M. J. Fairuz, Dr. Jae-Hun Yang, and A/Prof Nikki Verrills for their support and technical assistance.

6. References

[1] Sung H, Ferlay J, Siegel RL, et al. Global cancer statistics 2020: GLOBOCAN estimates of incidence and mortality worldwide for 36 cancers in 185 countries. CA: a cancer journal for clinicians. 2021;71(3):209-249.

[2] Herbst RS, Morgensztern D, Boshoff C. The biology and management of non-small cell lung cancer. Nature. 2018;553(7689):446-454.

[3] Chaft JE, Rimner A, Weder W, et al. Evolution of systemic therapy for stages I–III non-metastatic non-small-cell lung cancer. Nature reviews Clinical oncology. 2021;18(9):547-557.

[4] Singh SS, Dahal A, Shrestha L, et al. Genotype driven therapy for non-small cell lung cancer: Resistance, pan inhibitors and immunotherapy. Current Medicinal Chemistry. 2020;27(32):5274-5316.

[5] Friedlaender A, Subbiah V, Russo A, et al. EGFR and HER2 exon 20 insertions in solid tumours: from biology to treatment. Nature reviews Clinical oncology. 2022;19(1):51-69.

[6] Passaro A, Jänne PA, Mok T, et al. Overcoming therapy resistance in EGFR-mutant lung cancer. Nature Cancer. 2021;2(4):377-391.

[7] Grant MJ, Herbst RS, Goldberg SB. Selecting the optimal immunotherapy regimen in driver-negative metastatic NSCLC. Nature reviews Clinical oncology. 2021;18(10):625-644.

[8] Jiang P, Geng L, Mao Z, et al. First-line chemotherapy plus immune checkpoint inhibitors or bevacizumab in advanced non-squamous non-small-cell lung cancer without EGFR mutations or ALK fusions. Immunotherapy. 2022;14(6):445-457.

[9] Wang J, Zhao Q, Cai L, et al. Efficacy of Bevacizumab and Gemcitabine in Combination with Cisplatin in the Treatment of Esophageal Cancer and the Effect on the Incidence of Adverse Reactions. BioMed Research International. 2022;2022.

[10] Nozawa K, Takatsuka D, Endo Y, et al. Association between bevacizumab with cancer drug therapies and drug-induced interstitial lung disease in patients with solid tumor: A systematic review and meta-analysis of randomised clinical trials. Critical Reviews in Oncology/Hematology. 2022;174:103703.

[11] Lu L, Zhan M, Li X-Y, et al. Clinically approved combination immunotherapy: Current status, limitations, and future perspective. Current research in immunology. 2022;3:118-127.

[12] Middleton G, Fletcher P, Popat S, et al. Publisher Correction: The National Lung Matrix Trial of personalised therapy in lung cancer. Nature. 2020;585(7826):E21-E21.

[13] Yuan M, Huang L-L, Chen J-H, et al. The emerging treatment landscape of targeted therapy in non-small-cell lung cancer. Signal transduction and targeted therapy. 2019;4(1):61.

[14] Drilon A, Hellmann MD. An umbrella approach to test lung cancer therapies. Nature. 2020;583(7818):688-689.

[15] Zugazagoitia J, Molina-Pinelo S, Lopez-Rios F, et al. Biological therapies in nonsmall cell lung cancer. European Respiratory Journal. 2017;49(3).

[16] Wan R, Dong X, Chen Q, et al. Efficacy and safety of MIL60 compared with bevacizumab in advanced or recurrent non-squamous non-small cell lung cancer: a phase 3 randomised, double-blind study. EClinicalMedicine. 2021;42.

[17] Nogami N, Barlesi F, Socinski MA, et al. IMpower150 final exploratory analyses for atezolizumab plus bevacizumab and chemotherapy in key NSCLC

patient subgroups with EGFR mutations or metastases in the liver or brain. Journal of Thoracic Oncology. 2022;17(2):309-323.
[18] Jenab-Wolcott J, Giantonio BJ. Bevacizumab: current indications and future development for management of solid tumors. Expert opinion on biological therapy. 2009;9(4):507-517.
[19] García-Fernández C, Fornaguera C, Borrós S. Nanomedicine in non-small cell lung cancer: From conventional treatments to immunotherapy. Cancers. 2020;12(6):1609.
[20] Wilhelm S, Tavares AJ, Dai Q, et al. Analysis of nanoparticle delivery to tumours. Nature reviews materials. 2016;1(5):1-12.
[21] Kwon S, Singh RK, Perez RA, et al. Silica-based mesoporous nanoparticles for controlled drug delivery. Journal of tissue engineering. 2013;4:2041731413503357.
[22] Tiburcius S, Krishnan K, Jose L, et al. Egg-yolk core–shell mesoporous silica nanoparticles for high doxorubicin loading and delivery to prostate cancer cells. Nanoscale. 2022;14(18):6830-6845.
[23] Vinu aA, Murugesan V, Hartmann M. Adsorption of lysozyme over mesoporous molecular sieves MCM-41 and SBA-15: influence of pH and aluminum incorporation. The Journal of Physical Chemistry B. 2004;108(22):7323-7330.
[24] Miyahara M, Vinu A, Hossain KZ, et al. Adsorption study of heme proteins on SBA-15 mesoporous silica with pore-filling models. Thin Solid Films. 2006;499(1-2):13-18.
[25] Ariga K, Ji Q, Hill JP, et al. Coupling of soft technology (layer-by-layer assembly) with hard materials (mesoporous solids) to give hierarchic functional structures. Soft Matter. 2009;5(19):3562-3571.
[26] Vinu A, Streb C, Murugesan V, et al. Adsorption of cytochrome c on new mesoporous carbon molecular sieves. The Journal of Physical Chemistry B. 2003;107(33):8297-8299.
[27] Chandrasekar G, Vinu A, Murugesan V, et al. Adsorption of vitamin E on mesoporous silica molecular sieves. Studies in Surface Science and Catalysis. Vol. 158: Elsevier; 2005. p. 1169-1176.
[28] Hun Kim M, Choi G, Elzatahry A, et al. Review of clay-drug hybrid materials for biomedical applications: Administration routes. Clays and Clay Minerals. 2016;64(2):115-130.
[29] Kumar R, Mondal K, Panda PK, et al. Core–shell nanostructures: perspectives towards drug delivery applications. Journal of Materials Chemistry B. 2020;8(39):8992-9027.
[30] Rong J, Li P, Ge Y, et al. Histone H2A-peptide-hybrided upconversion mesoporous silica nanoparticles for bortezomib/p53 delivery and apoptosis induction. Colloids and Surfaces B: Biointerfaces. 2020;186:110674.
[31] Almáši M, Beňová E, Zeleňák V, et al. Cytotoxicity study and influence of SBA-15 surface polarity and pH on adsorption and release properties of anticancer agent pemetrexed. Materials Science and Engineering: C. 2020;109:110552.
[32] Wang T, Liu Y, Wu C. Effect of paclitaxel-mesoporous silica nanoparticles with a core-shell structure on the human lung cancer cell line A549. Nanoscale research letters. 2017;12:1-8.
[33] Cho N-H, Cheong T-C, Min JH, et al. A multifunctional core–shell nanoparticle for dendritic cell-based cancer immunotherapy. Nature nanotechnology. 2011;6(10):675-682.

[34] Junginger H. Oral applications of pulsatile drug delivery. PAPERBACK APV. 1993;33:113-113.
[35] Streubel A, Siepmann J, Peppas N, et al. Bimodal drug release achieved with multi-layer matrix tablets: transport mechanisms and device design. Journal of Controlled Release. 2000;69(3):455-468.
[36] Radhakrishnan D, Mohanan S, Choi G, et al. The emergence of nanoporous materials in lung cancer therapy. Science and technology of advanced materials. 2022;23(1):225-274.
[37] Sundarraj S, Thangam R, Sujitha MV, et al. Ligand-conjugated mesoporous silica nanorattles based on enzyme targeted prodrug delivery system for effective lung cancer therapy. Toxicology and applied pharmacology. 2014;275(3):232-243.
[38] Tiburcius S, Krishnan K, Patel V, et al. Triple surfactant assisted synthesis of novel core-shell mesoporous silica nanoparticles with high surface area for drug delivery for prostate cancer. Bulletin of the Chemical Society of Japan. 2022;95(2):331-340.
[39] Zhang L, Song F, Wu Y, et al. A novel amino and carboxyl functionalised mesoporous silica as an efficient adsorbent for nickel (II). Journal of Chemical & Engineering Data. 2018;64(1):176-188.
[40] Cauda V, Schlossbauer A, Kecht J, et al. Multiple core− shell functionalised colloidal mesoporous silica nanoparticles. Journal of the American Chemical Society. 2009;131(32):11361-11370.
[41] Zhang Y, Guo J, Zhang X-L, et al. Antibody fragment-armed mesoporous silica nanoparticles for the targeted delivery of bevacizumab in ovarian cancer cells. International journal of pharmaceutics. 2015;496(2):1026-1033.
[42] Malhotra B, Evans T, Weiss J, et al. Carboplatin/pemetrexed/bevacizumab in the treatment of patients with advanced non–small-cell lung cancer: a single-institution experience. Clinical Lung Cancer. 2010;11(3):192-197.
[43] Stefanou D, Stamatopoulou S, Sakellaropoulou A, et al. Bevacizumab, pemetrexed and carboplatin in first-line treatment of non-small cell lung cancer patients: focus on patients with brain metastases. Oncology Letters. 2016;12(6):4635-4642.
[44] Yan J, Zhong N, Liu G, et al. Usp9x-and Noxa-mediated Mcl-1 downregulation contributes to pemetrexed-induced apoptosis in human non-small-cell lung cancer cells. Cell death & disease. 2014;5(7):e1316-e1316.
[45] Pangeni R, Choi JU, Panthi VK, et al. Enhanced oral absorption of pemetrexed by ion-pairing complex formation with deoxycholic acid derivative and multiple nanoemulsion formulations: preparation, characterization, and in vivo oral bioavailability and anticancer effect. International Journal of Nanomedicine. 2018:3329-3351.
[46] Spitzmüller L, Nitschke F, Rudolph B, et al. Dissolution control and stability improvement of silica nanoparticles in aqueous media. Journal of Nanoparticle Research. 2023;25(3):40.
[47] Zhang D, Wei L, Zhong M, et al. Correction: The morphology and surface charge-dependent cellular uptake efficiency of upconversion nanostructures revealed by single-particle optical microscopy. Chemical Science. 2022;13(12):3610-3610.
[48] Fröhlich E. The role of surface charge in cellular uptake and cytotoxicity of medical nanoparticles. International journal of nanomedicine. 2012:5577-5591.

[49] Chen K-C, Yang T-Y, Wu C-C, et al. Pemetrexed induces S-phase arrest and apoptosis via a deregulated activation of Akt signaling pathway. PloS one. 2014;9(5):e97888.

Table 1. Brunauer–Emmett–Teller (BET) specific surface area, specific pore volume and pore diameter of all the @MSN-xF samples.

Sample Name	Surface Area S.A (m^2/g)	Pore Volume P.V(cm^3/g)	Pore Size PS (nm)
@MSN-0F	706	0.6	2.1, 3.7
@MSN-0.1F	710	0.4	1.9, 3.3
@MSN-0.2F	681	0.42	1.9, 3.4
@MSN-0.3F	695	0.46	2.0, 3.4
@MSN-0.5F	654	0.53	2.1, 3.5

Figure 1. HR-SEM images of 1A: @MSN-0F, 1B: @MSN-0.1F, 1C and 1D: @MSN-0.2F, 1E: @MSN-0.3F and 1F: @MSN-0.5F. Yellow arrow in 1A indicates formation of empty core-shell MSN.

Figure 2. 2A, 2B, 2C) HR-TEM images of @MSN-0F and 2D, 2E, 2F- HR-TEM images of @MSN-0.2F.

Figure 3. A) Powder XRD data, B) N_2 isotherms, and C) Pore size distribution (BJH) of @MSN-xF. D) FTIR spectra of @MSN-0.2F, NH_2@MSN, NH_2@MSN-CN and NH2@MSN-CO.

Figure 4. A) Thermogravimetric analysis of a) @MSN-0.2F, b) NH_2@MSN, c) NH_2@MSN-CO, d) PEM@MSN-NHCO, e) PEM@MSN, and f) PEM@MSN-NH. PEM = pemetrexed. B) Drug loading capacity (pemetrexed) of pristine and functionalised @MSN-0.2F.

Figure 5. Cumulative pemetrexed release from pristine and functionalised @MSN-0.2F in A) acetate buffer (pH=5.5) and B) phosphate buffer (pH=7.4). BEV = bevacizumab, PEM = pemetrexed.

Figure 7. Cell viability of @MSN-0.2F, NH_2@MSN, and NH_2@MSN-CO in A) A549 24 h, B) A549 48 h, C) PC9 24 h, D) PC9 48 h and PEM@MSN, PEM@MSN-NH, PEM@MSN-NHCO and BEV-PEM@MSN-NHCO in E) A549 24 h, F) A549 48 h, G) PC9 24 h and H) PC9 48 h. Green colour represents MSN and PEM@MSN. Yellow colour represents MSN-NH and PEM@MSN-NH. Blue colour represents MSN-NH-CO and PEM@MSN-NHCO and Pink colour indicates BEV-PEM@MSN-NHCO). Holm-Sidak was used to determine statistical significance (Shapiro-Wilk adjusted p-values). *$P \leq 0.05$; **$P \leq 0.01$; ***$P \leq 0.001$.

Figure 6. Flow cytometry analysis of the uptake of FITC-labelled MSN in A549 cells: A) without treatment (control) and with different concentrations of NH_2@MSN-CO and B) 50 μg/mL, C) 100 μg/mL, D) 150 μg/mL, E) 200 μg/mL and F) 300 μg/mL for 24 h.

Figure 8. Confocal images of FITC-labelled BEV-PEM@MSN in A549 cells at different time-points. A) 3 h B) 6 h C) 12 h, bars: 20 μm. Blue stain is the DAPI stained cell nuclei, green colour represents the FITC labelled drug-loaded nanoparticles, and orange colour stains the cell membrane.

Figure 9. Pemetrexed-induced apoptosis in A549 cells treated with 200 μg/mL of PEM@MSN-NHCO, A) 6 h; B) 12 h; and 200 μg/mL BEV-PEM@MSN C) 6 h; D) 12 h; A549 cells were stained with FITC-annexin/PI combination and analysed using 488 nm excitation with 530/30 nm and 575/24 nm bandpass filters at 100 μL min−1 collection rate.

Statement of Novelty

This study introduces novel core-shell hollow mesoporous silica nanoparticles with bimodal porosity, high drug loading, and versatile surface functionalization for enhanced targeted drug delivery in non-small cell lung cancer therapy.

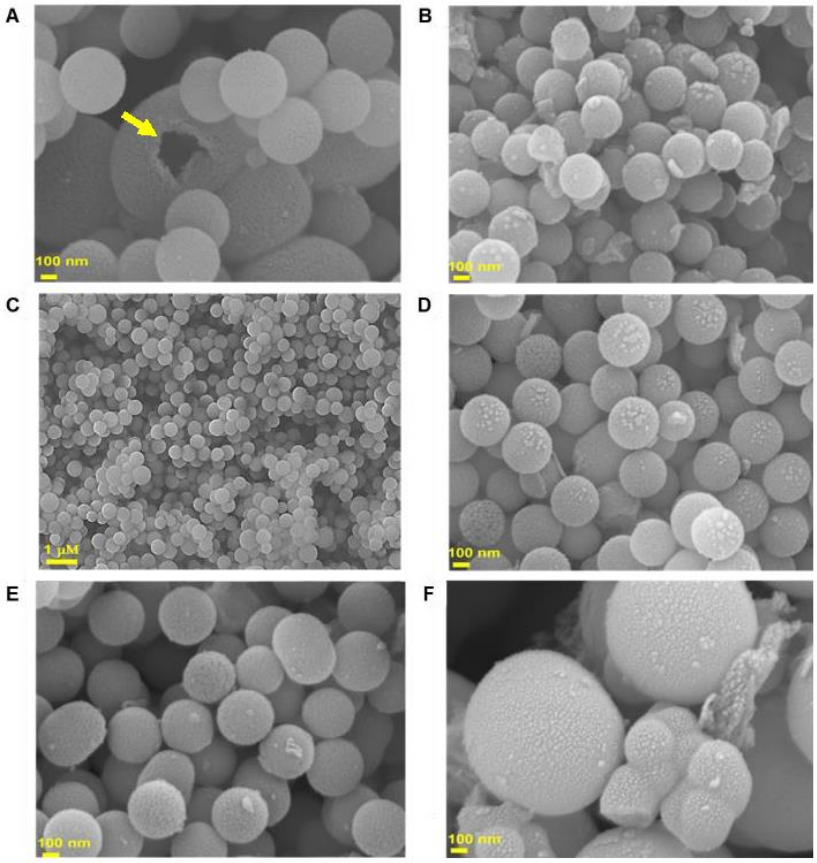
A
100 nm
B
100 nm
C
1 μM
D
100 nm
E
100 nm
F
100 nm

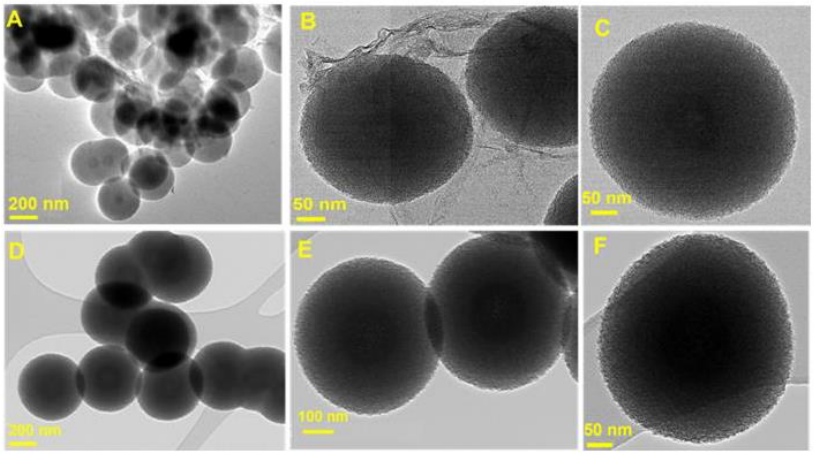
A
200 nm
B
50 nm
C
50 nm
D
200 nm
E
100 nm
F
50 nm

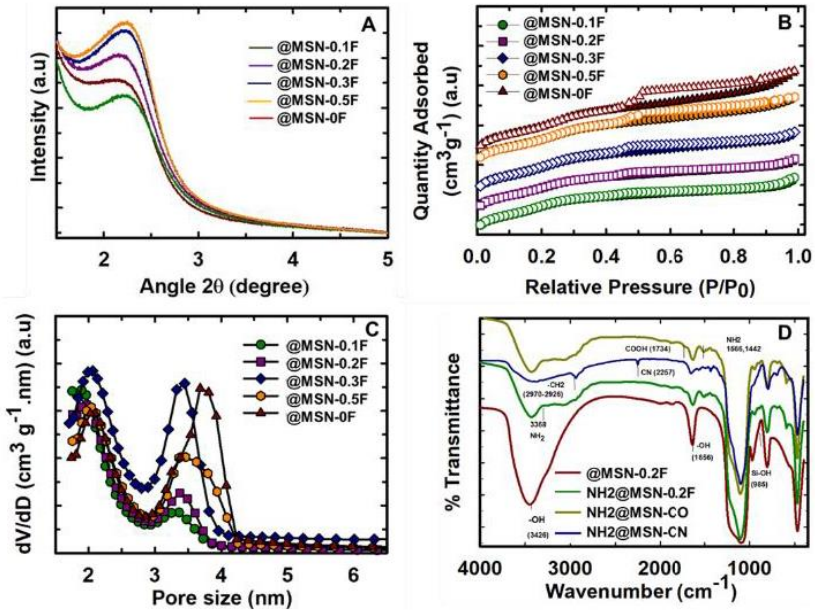
A
Intensity (a.u)
Angle 2θ (degree)
@MSN-0.1F
@MSN-0.2F
@MSN-0.3F
@MSN-0.5F
@MSN-0F
B
Quantity Adsorbed (cm3g-1) (a.u)
Relative Pressure (P/P0)
C
dV/dD (cm3 g-1 .nm) (a.u)
Pore size (nm)
D
% Transmittance
Wavenumber (cm-1)
@MSN-0.2F
NH2@MSN-0.2F
NH2@MSN-CO
NH2@MSN-CN
COOH (1734)
NH2 1566,1442
CN (2257)
-CH2 (2970-2926)
3368 NH2
-OH (1656)
Si-OH (988)
-OH (3426)

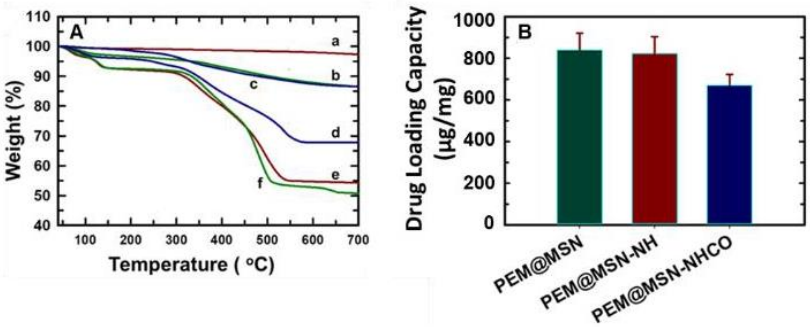
A
Weight (%)
Temperature (°C)
a
b
c
d
e
f
B
Drug Loading Capacity (μg/mg)
PEM@MSN
PEM@MSN-NH
PEM@MSN-NHCO

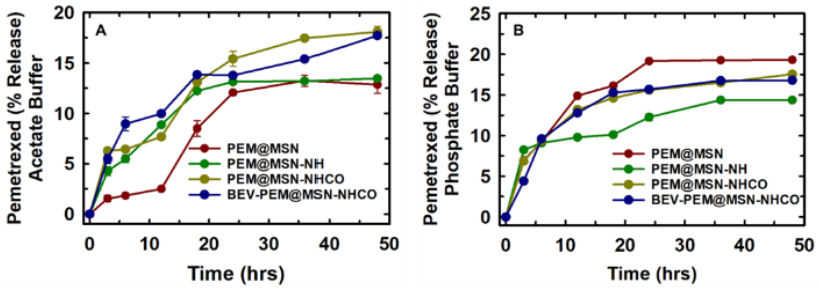
A
Pemetrexed (% Release)
Acetate Buffer
Time (hrs)
PEM@MSN
PEM@MSN-NH
PEM@MSN-NHCO
BEV-PEM@MSN-NHCO
B
Pemetrexed (% Release)
Phosphate Buffer
Time (hrs)
PEM@MSN
PEM@MSN-NH
PEM@MSN-NHCO
BEV-PEM@MSN-NHCO

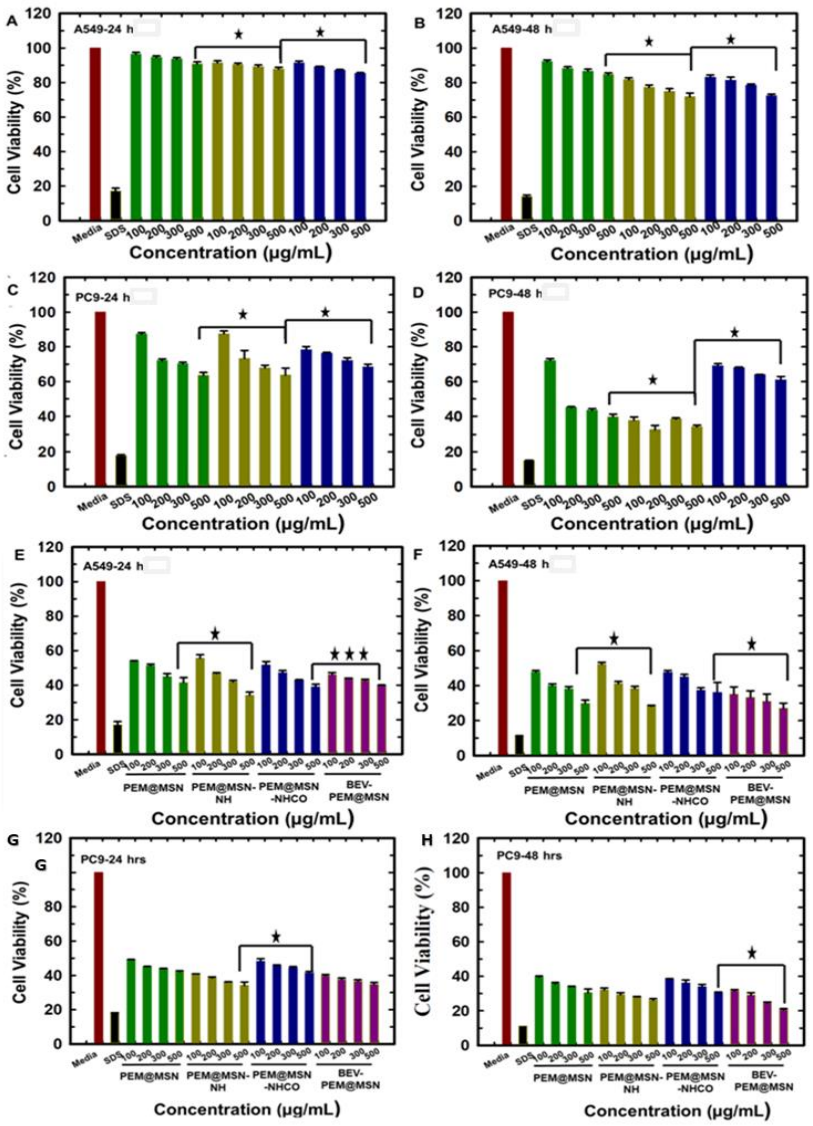
A
A549-24 h
Cell Viability (%)
Media
SDS
100
200
300
500
Concentration (μg/mL)
B
A549-48 h
C
PC9-24 h
D
PC9-48 h
E
A549-24 h
F
A549-48 h
PEM@MSN
PEM@MSN-NH
PEM@MSN-NHCO
BEV-PEM@MSN
G
PC9-24 hrs
H
PC9-48 hrs

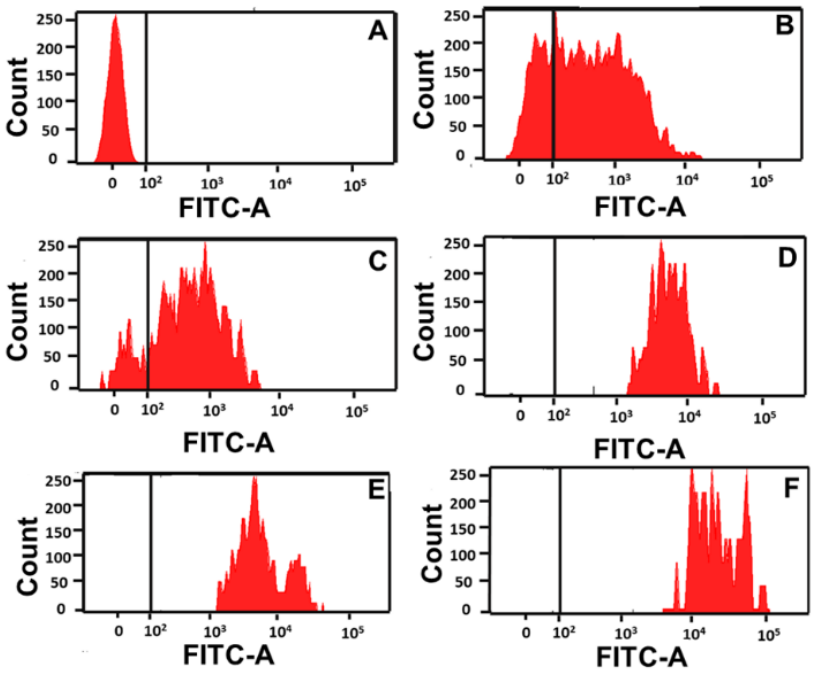
A
B
C
D
E
F
Count
FITC-A
250
200
150
100
50
0
0
10^2
10^3
10^4
10^5

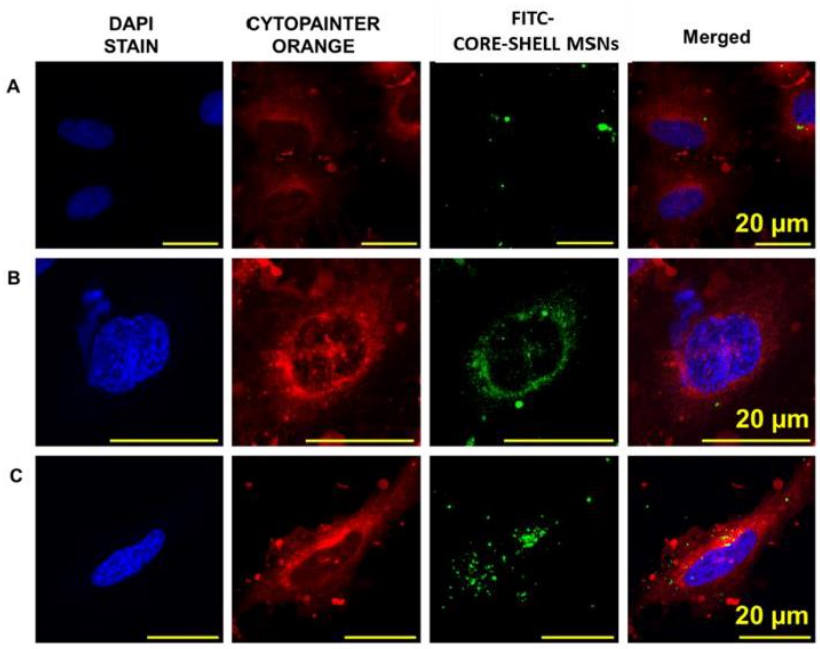
DAPI STAIN
CYTOPAINTER ORANGE
FITC-CORE-SHELL MSNs
Merged
A
B
C
20 µm
20 µm
20 µm

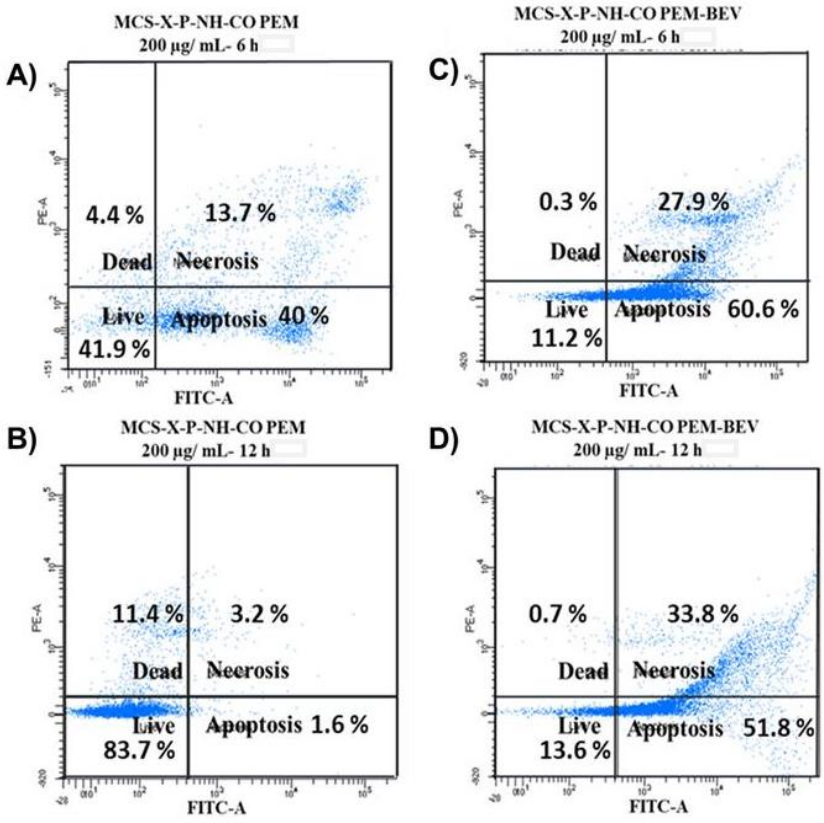
A)
MCS-X-P-NH-CO PEM
200 µg/ mL- 6 h
4.4 %
13.7 %
Dead
Necrosis
Live
Apoptosis 40 %
41.9 %
PE-A
FITC-A
C)
MCS-X-P-NH-CO PEM-BEV
200 µg/ mL- 6 h
0.3 %
27.9 %
Dead
Necrosis
Live
Apoptosis 60.6 %
11.2 %
PE-A
FITC-A
B)
MCS-X-P-NH-CO PEM
200 µg/ mL- 12 h
11.4 %
3.2 %
Dead
Necrosis
Live
Apoptosis 1.6 %
83.7 %
PE-A
FITC-A
D)
MCS-X-P-NH-CO PEM-BEV
200 µg/ mL- 12 h
0.7 %
33.8 %
Dead
Necrosis
Live
Apoptosis 51.8 %
13.6 %
PE-A
FITC-A

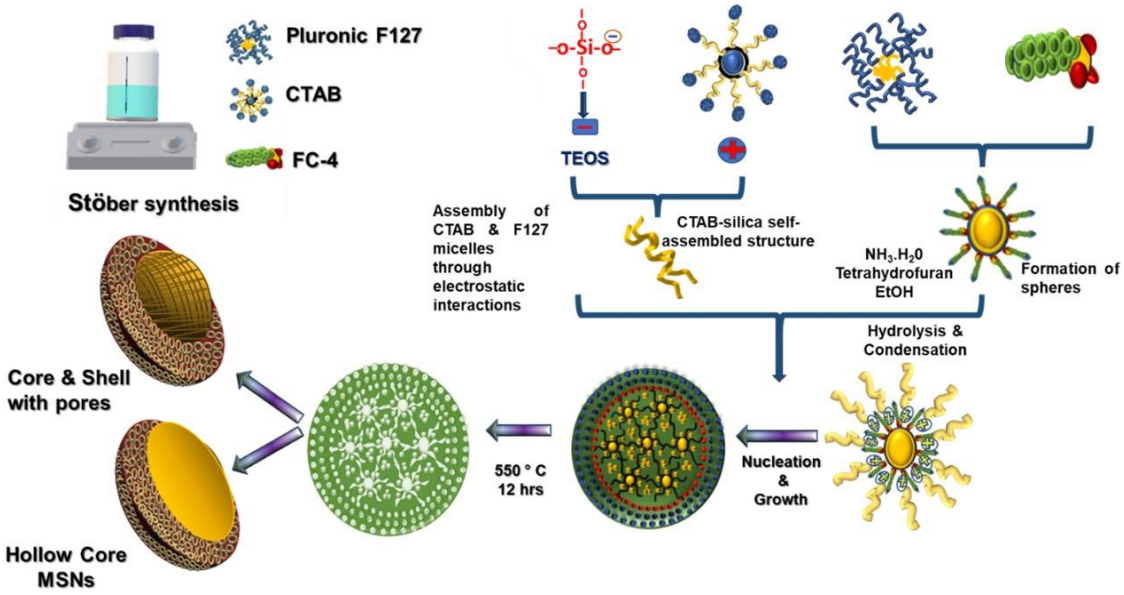

GA

Combinatorial treatment with bevacizumab functionalized pemetrexed loaded core-shell silica nanoparticles for enhanced anti-tumor efficacy in non-small cell lung cancer

Deepika Radhakrishnan[1], Vaishwik Patel[1], Shan Mohanan[1], Sharon Wong[1], Jacob Netherton[2], Ajay Karakoti[1], Ajayan Vinu[1]*

[1]*Global Innovative Center for Advanced Nanomaterials, The University of Newcastle, Callaghan, Australia*

[2]*School of Biomedical Sciences and Pharmacy, The University of Newcastle, Callaghan, Australia*

Contact: Ajayan Vinu: Ajayan.Vinu@newcastle.edu.au, Global Innovative Center for Advanced Nanomaterials, The University of Newcastle, Callaghan, Australia

Cellular Apoptosis:

The interpretation of the results involves the following: Annexin V-negative/PI-negative cells (lower left quadrant) represent live cells, Annexin V-positive and PI-negative cells (lower right quadrant) denote early apoptotic cells, Annexin V-positive and PI-positive cells (upper right quadrant) signify necrotic and late apoptotic cells, and Annexin V-negative and PI-positive cells (upper left quadrant) indicate necrotic cells.

Supplementary Figures and Tables

Table S1: Surface properties of the amine and carboxyl functionalised @MSN-0.2F.

Sample Name	Surface Area S.A (m^2/g)	Pore Volume P.V(cm^3/g)	Pore Size PS (nm)
@MSN-0.2F	681	0.42	3
NH_2@MSN	402	0.11	3.2
NH_2@MSN -CO	194	0.067	4.2

Table S2: CHNS analyzer has been used to confirm the detailed elemental analysis of Amine functionalized silica, Amine and carboxyl functionalized silica and Pemetrexed loaded amine and carboxyl functionalized silica.

CHNS ANALYSIS			
Sample Name	**Carbon**	**Hydrogen**	**Nitrogen**
NH_2@MSN	**7.52**	**2.32**	**2.92**
NH_2@MSN-CO	**5.37**	**1.76**	**1.96**
PEM@MSN-NHCO	**4.78**	**1.73**	**1.97**

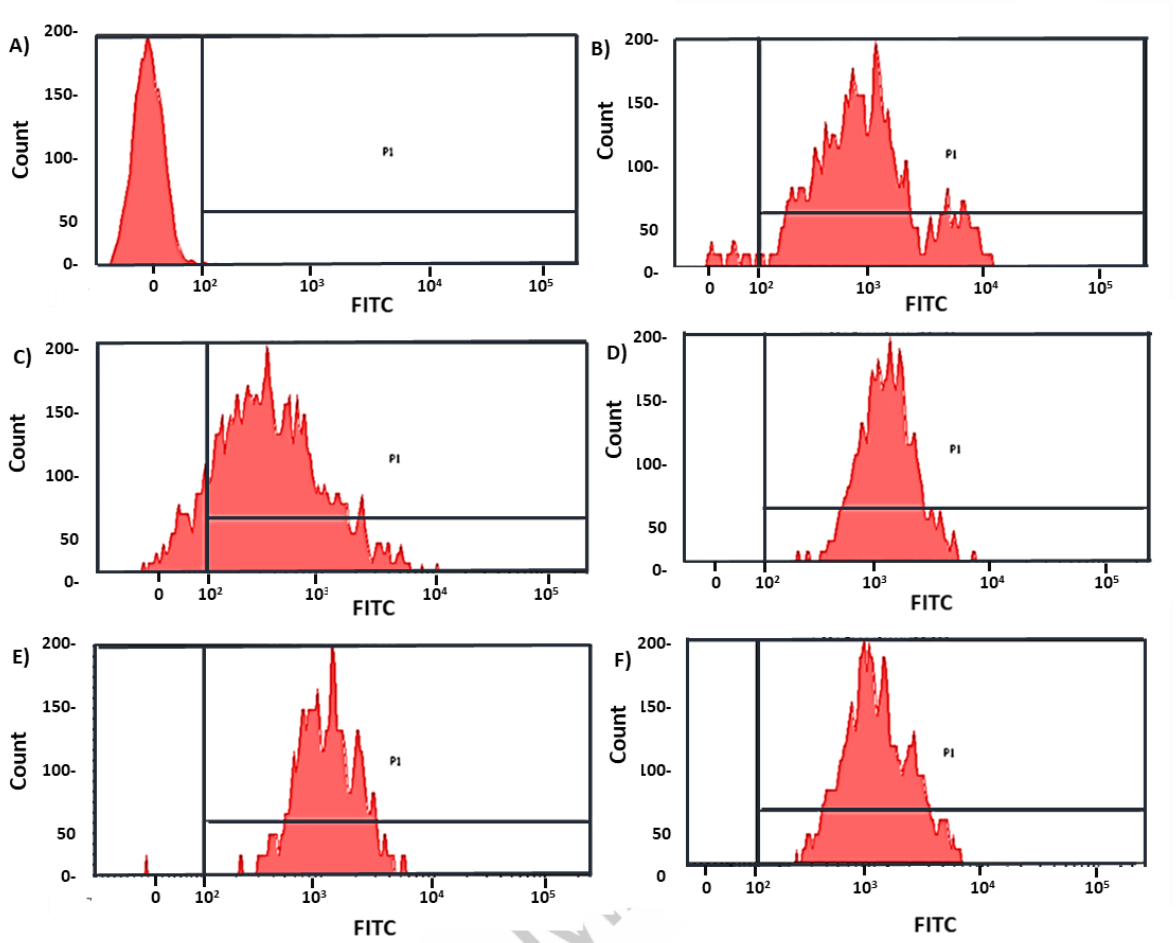

Figure S3: Flow cytometry analysis of the uptake of FITC-labelled MSN measured by flow cytometry in PC-9 cells of A) without treatment (control) and with different concentrations of NH_2@MSN-CO, B) 50 µg/mL, C) 100 µg/mL, D) 150 µg/mL, E) 200 µg/mL, and F) 300 µg/mL for 24 h.